Integrated and DC-powered superconducting microcomb

Chen-Guang Wang[1,2,3], Wuyue Xu[1,2,3], Chong Li[1,2,3], Lili Shi[1], Junliang Jiang[1], Tingting Guo[1], Wen-Cheng Yue[1,2,3], Tianyu Li[1,2,3], Ping Zhang[1], Yang-Yang Lyu[1,2], Jiazheng Pan[2], Xiuhao Deng[4,5], Ying Dong[6], Xuecou Tu[1,5], Sining Dong[1,3], Chunhai Cao[1], Labao Zhang[1,5], Xiaoqing Jia[1,5], Guozhu Sun[1,5], Lin Kang[1,5], Jian Chen[1,2], Yong-Lei Wang[1,2,3, *], Huabing Wang[1,2, *], Peiheng Wu[1,2, *]

[1] *Research Institute of Superconductor Electronics, School of Electronic Science and Engineering, Nanjing University, Nanjing, China*
[2] *Purple Mountain Laboratories, Nanjing, China*
[3] *National Key Laboratory of Spintronics, Nanjing University, Suzhou, China*
[4] *Shenzhen Institute for Quantum Science and Engineering, Southern University of Science and Technology, Shenzhen, China*
[5] *Hefei National Laboratory, Hefei, China*
[6] *College of Metrology Measurement and Instrument, China Jiliang University, Hangzhou, China*

* Correspondence to: yongleiwang@nju.edu.cn; hbwang@nju.edu.cn; phwu@nju.edu.cn

Abstract

Frequency combs, specialized laser sources emitting multiple equidistant frequency lines, have revolutionized science and technology with unprecedented precision and versatility. Recently, integrated frequency combs are emerging as scalable solutions for on-chip photonics. Here, we demonstrate a fully integrated superconducting microcomb that is easy to manufacture, simple to operate, and consumes ultra-low power. Our turnkey apparatus comprises a basic nonlinear superconducting device, a Josephson junction, directly coupled to a superconducting microstrip resonator. We showcase coherent comb generation through self-started mode-locking. Therefore, comb emission is initiated solely by activating a DC bias source, with power consumption as low as tens of picowatts. The resulting comb spectrum resides in the microwave domain and spans multiple octaves. The linewidths of all comb lines can be narrowed down to 1 Hz through a unique coherent injection-locking technique. Our work represents a critical step towards fully integrated microwave photonics and offers the potential for integrated quantum processors.

Introduction

Frequency combs serve as high-precision rulers for frequency and time measurement, playing a pivotal role in a wide variety of modern science and technologies [1-5], including optical clocks, LIDAR, spectroscopy, arbitrary waveform generation, and optical neural networks. Over the past two decades, integrated combs have garnered significant research interests [5-18], leading to miniaturized and chip-based photonic systems [7]. However, most on-chip frequency combs, such as integrated semiconductor mode-locked lasers and microresonator-based Kerr combs, mainly operate in the optical frequency domain. A fully integrated frequency comb functioning in the microwave domain remains elusive, impeding the advancement of chip-based microwave spectroscopy and integrated quantum circuits, which typically require precise microwave control. Here, we address these challenges by introducing an all-superconductor-based microcomb, featuring an elegantly simple structure, effortless operation, and ultra-low power consumption.

Our superconducting frequency comb is fully integrated, comprising two fundamental superconductor devices: a Josephson junction directly coupled to a superconducting coplanar waveguide (CPW) resonator, as illustrated in Fig. 1a (see Supplementary Figure 1 for a photo of our device). Device fabrication is achieved through straightforward procedures utilizing standard photolithography and electron beam evaporation techniques (See Methods). The Josephson junction consists of two superconductors connected by a weak link or a thin insulating barrier. It acts as an ideal voltage-to-frequency converter, emitting photons at the Josephson frequency $f_J = 2eV_{dc}/h$, where $2e$ is the charge of a Cooper pair, V_{dc} is the DC voltage bias across the junction, and h is Planck's constant. Meanwhile, the superconducting CPW resonator is another crucial superconductor device widely used in high-sensitive detectors and circuits for qubit control and read-out [19]. We demonstrate that the combination of these two fundamental superconducting elements can generate a coherent frequency comb (Fig. 1b and 1c). Its on-chip generation of pulse waves and inherent compatibility with production, operation, and integration into circuit quantum electrodynamics [20-22] offers the potential for miniaturized, low-cost, and energy-efficient quantum processors.

The Josephson junction coupled superconducting resonator has drawn significant research interest due to its capability not only to operate as ultrasensitive sensors, such as for single photon detection [23] and/or thermometry [24], but also to function as a coherent photon source [25-34]. Particularly, in the strong coupling regime, the device generates stable microwave lasing [25] and demonstrates remarkably low noise [26]. However, in previous investigations, the coupled devices were all operated in single mode, resulting in continuous-wave emissions. Their properties under a multimode operation have not been explored.

Results

Coherent comb generation. We demonstrate that a Josephson junction coupled to a

superconducting resonator can generate a self-phase-locked coherent frequency comb under *multimode* operation. The coupling between a Josephson junction and a resonator is proportional to the Josephson energy $E_J \equiv hI_c/2e$, where I_c is superconducting critical current [25, 28]. To directly ensure strong coupling, we employ a Josephson junction with a large I_c. This is achieved by fabricating a sizable Josephson junction (approximately 4 µm^2), resulting in a relatively large supercurrent of $I_D \approx 2$ µA in the lasing state (Fig. 1b), which surpasses by more than two orders of magnitude compared to that in the continuous-wave Josephson laser [25]. To achieve multimode operation within the frequency range of interest (typically 1~10 GHz), we fabricate a superconducting resonator with a low free spectrum range of 0.75 GHz. The strong coupling allows stable microwave lasing when a dc voltage bias $V_{dc} \geq 20$ µV is applied to the Josephson junction (Fig. 1b).

Figure 1c shows the comb spectrum measured at V_{dc}=43 µV. First, we will prove that the observed spectrum in Fig. 1c indeed represents a coherent frequency comb. The raised background between 3~10 GHz in Fig. 1c is a consequence of the limited bandwidth of amplifiers. Therefore, our subsequent investigations will focus on the frequency range in the detection bandwidth. The frequencies of a comb are given by the formula: $f_m = f_0 + mf_r$, where f_0 denotes the carrier offset frequency, f_r represents the repetition frequency, and m stands for the mode number [1-5]. The extracted mode frequencies are shown in Fig. 1d, align perfectly with fitting to the comb formula. The result indicates a negligible offset frequency ($f_0 \approx 0$ GHz). Consequently, our superconducting microcomb can be expressed by a simplified comb formula:
$$f_m = mf_r \qquad (1)$$
Additionally, Figures 1c and 1d demonstrate that the repetition frequency f_r nicely aligns with the free spectrum range (0.75 GHz) of the half-wave resonator.

The evenly spaced spectral lines alone are not sufficient for correlations among the comb teeth. To examine the coherence state of the emitted signal, we firstly proved that each individual mode has a stable phase using the heterodyne detection technique (Supplementary Figure 2). One direct consequence of phase-coherent comb is the generation of pulses in the time domain [1-5]. Figure 2a displays a comb spectrum, and its corresponding time-dependent waveform is shown in Figs. 2b and 2c. The waveform reveals a sequence of microwave pulses, indicating that all spectrum modes are phase-locked and maintain a stable phase relationship. Moreover, every pulse displays identical features, as seen in Fig. 2d by the perfect overlap of two pulse-waves. This indicates that all pulses are in-phase, and also suggests a carrier offset frequency of 0 Hz, thus confirming that all the spectral lines share a uniform phase. The coherence of the comb modes can be further validated through a unique coherent injection locking effect, as demonstrated below.

The emission power of each individual comb line, ranging up to subpicowatt (see Supplementary Figure 3), is consistent with that of the continuous-wave (or single-mode) source [25]. The microcomb's performance could be further enhanced by refining the structures and parameters of the Josephson junction-coupled resonators [26]. The stability of the frequency comb is determined by the linewidth of the spectral lines (see Supplementary Figure 4). In general, the overall linewidth is influenced by the quality factor of the resonator, the stability of the DC bias voltage, and environmental electromagnetic and thermal noise. Moreover, our experiments demonstrate that the linewidth of our comb increases quadratically with the mode number (or frequency), as illustrated in Supplementary Figure 5. This finding is consistent with the observations in quantum-

limited optical combs [35, 36].

Coherent injection locking effect. Injection-locking is a widely used technique for effectively narrowing the linewidth of a laser source [25, 26, 37, 38]. In optical frequency combs, it has been demonstrated only in a few cases in quantum cascade lasers by injecting a radio-frequency (RF) modulation at the cavity roundtrip frequency [39-42]. In our superconducting microcomb, we showcase a distinct coherent injection locking effect that can be achieved by injecting an external microwave at any arbitrary comb mode. For instance, we select an arbitrary mode, such as $m_{inj} = 7$, as the injection tone (Fig. 3a). Then, an injection signal f_{inj} is applied and swept around f_7=5.26 GHz. We measure the spectra at frequencies f_{sen} around various sensing modes m_{sen} (Fig. 3a). The resulting spectra maps are illustrated in Figs. 3b-3d (additional results in Supplementary Figure 6). We find that all modes are simultaneously locked within the same injection frequency range Δf_{inj}=8.08 MHz (see Figs. 3b and 3d for definition and Fig. 3k for extracted values). This reaffirms that all spectral lines are coherently phase-locked.

This unique coherent injection-locking effect results in an ultra-high-resolution comb, with the linewidth of all comb teeth significantly narrowed down to ≤ 1 Hz, as shown in Figs. 3e-3g and their insets. It's worth noting that the observed linewidth of 1 Hz is constrained by the resolution bandwidth of the spectrum analyzer used in the experiments [26], implying the potential for even narrower linewidths.

The injection-locking range Δf_{inj} of our microcomb widens with the injection power P_{inj} (Supplementary Figure 7). Specifically, when $m_{sen}=m_{inj}$ (Figs. 3c, 3f, and 3i), the injection-locking phenomena replicate those observed in the continuous-wave source [25, 26], and can therefore be explained by the Adler's theory [43]. However, the results for the comb modes with $m_{sen} \neq m_{inj}$ cannot be described by the Adler's equation (see Supplementary Figures 8a and 8b). We find that the locked sensing frequency range Δf_{sen} (see Figs. 3b-3d for definition) is proportional to m (Fig. 3l). This implies that the radiation frequencies of the injection-locked comb satisfy the comb formula (1) over the entire locked frequency range. Consequently, this introduces an in-situ tunable superconducting microcomb, allowing for adjustable f_r within the range of $\Delta f_{inj}/m_{inj}$.

The coherent injection-locking leads to a unique frequency-pulling effect, particularly noticeable when $m_{sen} \neq m_{inj}$. Figures 3h-3j illustrate these effects when f_{inj} is fixed at an off-resonance tone (the corresponding on-resonance injection results are shown in Supplementary Figure 9), shifted from the free-running emission tone by $\Delta f_{off} = 8$ MHz. When $m_{sen} = m_{inj}$, the emission line is gradually pulled toward f_{inj} with increasing injection power P_{inj}, ultimately locking at f_{inj} (Fig. 3i). This behavior mirrors that observed in a continuous-wave source [25, 26]. However, the remarkable outcome arises when $m_{sen} \neq m_{inj}$. In this case, although no injection tone is applied around each sensing mode, notable emission lines are induced at the corresponding tones, termed 'induced-injection tone' and labeled as f_{id} in Figs. 3b, 3d, 3h, and 3j. The linewidth of the f_{id} lines is considerably narrower than those of the free-running emissions and the side-band harmonics (see Supplementary Figure 10). Furthermore, neither f_{id} emission nor Kerr comb generation are observed with RF injection under zero DC bias-voltage (Supplementary Figure 11). These indicate that the f_{id} emissions originate from the mutual interactions among Josephson photons, injection photons, and the resonator's multi-modes, setting the f_{id} signals apart from the Kerr combs generated directly from RF pumping [44].

4

When $m_{sen} \neq m_{inj}$, as depicted in Figs. 3h and 3j, while the emissions of all the modes are pulled toward f_{id} tones with increasing P_{inj}, the f_{id} tones themselves also shift with P_{inj}. Consequently, this results in the locked frequency range $\Delta f_{lock} \neq \Delta f_{off}$ (see Figs. 3h and 3j). Figure 3m demonstrates that Δf_{lock} is also proportional to m with $\Delta f_{lock} = \dfrac{m}{m_{inj}} \Delta f_{off}$, perfectly aligned with the requirements of the comb formula (1) for the emissions within the locking range.

There is no existing theory that can describe our observed coherent injection-locking effect. We have derived an extended Adler's equation to quantitatively describe these unique phenomena. As analyzed above, in the locking range Δf_{inj}, all comb emissions are described by the comb formula (1). In the unlocking range outside Δf_{inj}, the emission signals are given by (please refer to Method for detailed derivation):

$$f_{m,n} = \frac{m}{m_{inj}}(f_{inj} + f_h) + n f_h \qquad (2)$$

Here, f_h denotes the repetition frequency of the harmonic emissions induced by off-resonance injection, and $n f_h$ represents the nth harmonic shift. The f_h is given by:

$$f_h = (f_{m_{inj}} - f_{inj})\sqrt{1 - (\frac{\Delta f_{inj}/2}{f_{m_{inj}} - f_{inj}})} \quad (3)$$

where $\Delta f_{inj} = \alpha\sqrt{P_{inj}}$ (with α as a constant related to cavity losses), and $f_{m_{inj}}$ is the mode frequency at m_{inj}. Notably, when $m = m_{inj}$, the extended Alder's equation (2) reduces to the standard Alder's equation. The perfect fittings in Figs. 3b-3d and 3h-3j indicate that our extended Alder's equation (2) accurately describes all the coherent injection-locking effects in our superconducting microcomb.

In previous studies of continuous-wave superconducting lasers, the down-conversion of higher-order Josephson frequencies to resonator's fundamental mode has been demonstrated [25]. However, the up-conversion of Josephson photons to higher mode has not been reported. In Fig. 4a, we present a comb spectrum (red) within our typical experimental bandwidth 3~10 GHz. The applied DC bias voltage across the Josephson junction is V_{dc}=36.387 µV, corresponding to a Josephson frequency $f_J = 17.60$ GHz. As illustrated in Fig. 4a, all the comb modes with $f_m < f_J$ are generated through down-conversion, and any modes with $f_m > f_J$ (if existing) would result from up-conversion. However, emissions with $f_m > 17.60$ GHz lie beyond the bandwidth of our spectrum measurements, preventing their direct observation.

The coherent injection-locking effect provides an advanced methodology for sensing comb emissions beyond the detection bandwidth. To demonstrate this, we perform injection-locking measurements using various injection tones with $m_{inj} = 1, 6, 54$, as illustrated in Fig. 4a, while selecting a fixed sensing tone within the detection bandwidth, such as $m_{sen} = 7$. Figures 4b-4d display the coherent injection-locking effects. The injection locking phenomenon arises from nonlinear interaction between emission tone and external injection signal [43]. Since no injection signal is applied at $m = 7$, the coherence injection locking effect displayed in Fig. 4d suggests the presence of a comb emission tone at $f_{54} = 39.28$ GHz, which is significantly higher than the Josephson frequency f_J=17.6 GHz. This observation provides evidence for the up-conversion process of Josephson photons to higher modes. The presence of comb emissions at $m = 1$ (Fig. 4b) and 54 (Fig. 4d) indicates that our Josephson microcomb spans a frequency range exceeding five

octaves, a span typically challenging to achieve in semiconductor-based frequency combs. It is essential to note that this octave value is limited by the upper-frequency limit of the microwave generator used in our experiments. Hence, it is highly likely that even higher modes could exist beyond this range.

Discussion

We have demonstrated a fully integrable superconducting microcomb. Unlike previously reported superconductor-based frequency combs [44-52], which all operated under microwave pumping using externally supplied, expensive, and energy-consuming microwave sources, our superconducting microcomb is driven solely by a DC bias voltage. This makes it highly desirable for scalable and on-chip integration. The initiation of our microcomb requires simply tuning on a low-power DC bias source, with a minimal input power as low as 40 pW (Fig. 1b)—approximately nine orders of magnitude lower than the semiconductor-based frequency combs. This presents significant advancement for ultrasensitive and energy-efficient applications.

The exceptional coherence of our comb enables a unique coherent injection-locking effect previously inaccessible in frequency combs, leading to an ultra-high-resolution and tunable comb. This innovation introduces unique functionalities, such as the generation of coherent subcombs through four-wave mixing, as showcased in Supplementary Figure 12. The simultaneous up- and down-conversion of Josephson photons significantly expands the comb's frequency range over multiple octaves. These capabilities offer added flexibility and tunability for applications of superconducting microcomb technology.

This DC-biased superconducting microcomb with ultra-low power consumption (down to a few tens of picowatts) can work at ultralow temperatures, aligning seamlessly with the operating conditions of superconducting quantum circuits. For a typical dilution refrigerator, which has a cooling power of hundreds of microwatts at 20 mK, in principle it is feasible to integrate up to millions of the combs at the base temperature based on their energy efficiency. Our comb can serve as a multifrequency microwave source for multiplexed quantum measurement [53]. An important potential application of our superconducting microcomb is the development of a low-cost, on-chip arbitrary waveform generator. This could be achieved by controlling the intensities of the comb teeth [54], which is possible by integrating our superconducting comb with a series of frequency-tunable superconducting resonators serving as adjustable filters [55]. This advancement promises substantial benefits for future quantum technologies. Moreover, implementing superconducting frequency combs in the terahertz domain could be feasible by using intrinsic Josephson junctions in high-temperature superconductors [56]. This approach could also extend the technology's working temperature range.

Methods

Device fabrication

We fabricated four superconducting microcombs (#1-#4), and detailed parameters are listed in Supplementary Tables 1. The superconducting resonators are fabricated using a superconducting Nb film for device #1 and a Ta (α-phase) film [57] for devices #2, #3, and #4. The film was sputtered on a 10 mm by 10 mm sapphire substrate (C-plane, thickness 650 µm). Standard photolithography followed by reactive ion etching in a CF4 was then used to define the resonators. The Al/AlO$_x$/Al (Al thicknesses 40 nm/80 nm) Josephson junction was fabricated using standard double-angle evaporation and lift-off techniques. To ensure good electrical contact between the Josephson junction and the resonator layers, the sample was ion-beam milled to remove residual oxides and resist residue from the surface of the resonator before the double-angle evaporation.

Experiments

The devices are mounted in a dilution refrigerator with a base temperature of 20 mK. A complete circuit is shown in Supplementary Figure 13. We adopt a similar approach to Refs. [25, 30,31] for the low noise biasing scheme to measure the tunneling current and provide a stable voltage bias to the device. The bias voltage is supplied by an on-chip voltage divider circuit consisting of a 10 Ω shunt resistor and a 10 Ω reference resistor. The current through the device is then measured via the voltage drop V_r across the 10 Ω reference resistor. The current I_D and voltage V_{dc} of the device is given by $I_D = V_r/10$ and $V_{dc} = 10I_{bias} - 20I_D$. Here, V_r is obtained from a nano voltmeter (Keithley 2182A) and I_{bias} is the output from a current source (Keithley 6221). Additional filtering for the circuit is provided by two 100 µF chip capacitors. Additionally, all low frequency lines are heavily filtered outside the PCB with multi-pole RC and PI low pass filters located on the mixing chamber of the dilution refrigerator.

The device's output signal is amplified by an amplifier chain consisting of a cryogenic amplifier (+42 dB) and two room-temperature amplifiers (+32 dB). The spectra are acquired by an Agilent N9010A spectrum analyzer (S/A) and the waveforms are recorded using a Keysight MSOV334A digital oscilloscope (D/O). The injection signal to the resonator is generated by an Agilent N5183A analog signal generator (S/G) and is attenuated by a low-temperature attenuation chain to assure that the thermal contribution of photons to the cavity is negligible.

Extended Adler's equation

In the unlocking range outside Δf_{inj}, the emission signals for $m_{sen}=m_{inj}$, which can be described by Adler's theory [43], are given by:

$$f_{m_{inj},n} = (f_{inj} + f_h) + nf_h \qquad (3)$$

where f_h is the repetition frequency of the harmonic emissions. The first term, $f_{inj} + f_h$, accounts for the comb's emission at m_{inj}, while nf_h represents the nth harmonic shift. The f_h is given by:

$$f_h = (f_{m_{inj},0} - f_{inj}) \sqrt{1 - (\frac{\Delta f_{inj}/2}{f_{m_{inj},0} - f_{inj}})}$$

where $\Delta f_{inj} = \alpha \sqrt{P_{inj}}$ (with α as a constant related to cavity losses). The comb's emission at m_{inj} corresponds to $n=0$, therefore we obtain $f_{m_{inj},0} = f_{inj} + f_h$ from equation (3). Utilizing the superconducting microcomb formula (1) (see the main text), we can express the comb's emissions for any arbitrary m as $f_{m,0} = \frac{m}{m_{inj}} f_{m_{inj},0} = \frac{m}{m_{inj}} (f_{inj} + f_h)$. By adding the nth harmonic shift $n f_h$, we derive an extended Adler's equation (2), as shown in the main text, for the coherent injection-locking in our superconducting combs.

DATA AVAILABILITY

All the data that support the findings of this study are available on the public repository

https://doi.org/10.6084/m9.figshare.25480621

References

[1] T. J. Kippenberg, R. Holzwarth, and S. A. Diddams. Microresonator-based optical frequency combs. *Science* **332**, 555 (2011).

[2] Nathalie Picqué and Theodor W. Hänsch. Frequency comb spectroscopy. *Nature Photon.* **13**, 146-157 (2019).

[3] Tare Fortier and Esther Baumann. 20 years of developments in optical frequency comb technology and applications. *Commun. Phys.* **2**,153 (2019).

[4] Scott A. Diddams, Kerry Vahala, and Thomas Udem. Optical frequency combs: Coherently uniting the electromagnetic spectrum. *Science* **369**, 267 (2020).

[5] Lin Chang, Songtao Liu, and John E. Bowers. Integrated optical frequency comb technologies. *Nature Photon.* **16**, 95-108 (2022).

[6] Qiushi Guo, Benjamin K. Gutierrez, Ryoto Sekine, Robert M. Gray, James A. Williams, Luis Ledezma, Luis Costa, Arkadev Roy, Selina Zhou, Mingchen Liu, Alireza Marandi. Ultrafast mode-locked laser in nanophotoniclithium niobate. *Science* **382**, 708-713 (2023).

[7] Haowen Shu, Lin Chang, Yuansheng Tao, Bitao Shen, Weiqiang Xie, Ming Jin, Andrew Netherton, Zihan Tao, Xuguang Zhang, Ruixuan Chen, Bowen Bai, Jun Qin, Shaohua Yu, Xingjun Wang, and John E. Bowers. Microcomb-driven silicon photonic systems. *Nature* **605**, 457–463 (2022).

[8] Chao Xiang, Junqiu Liu, Joel Guo, Lin Chang, Rui Ning Wang, Wenle Weng, Jonathan Peters, Weiqiang Xie, Zeyu Zhang, Johann Riemensberger, Jennifer Selvidge, Tobias J. Kippenberg, John E. Bowers. Laser soliton microcombs heterogeneouslyintegrated on silicon. *Science* **373**, 99-103 (2021).

[9] Tobias J. Kippenberg, Alexander L. Gaeta, Michal Lipson, Michael L. Gorodetsky. Dissipative Kerr solitons in optical microresonators. *Science* **361**, 567 (2018).

[10] Xingyuan Xu, Mengxi Tan, Bill Corcoran, Jiayang Wu, Andreas Boes, Thach G. Nguyen, Sai T. Chu, Brent E. Little, Damien G. Hicks, Roberto Morandotti, Arnan Mitchell & David J. Moss. 11 TOPS photonic convolutional accelerator for optical neural networks. *Nature* **589**, 44–51 (2021).

[11] J. Feldmann, N. Youngblood, M. Karpov, H. Gehring, X. Li, M. Stappers, M. Le Gallo, X. Fu, A. Lukashchuk, A. S. Raja, J. Liu, C. D. Wright, A. Sebastian, T. J. Kippenberg, W. H. P. Pernice & H. Bhaskaran. Parallel convolutional processing using an integrated photonic tensor core. *Nature* **589**, 52–58 (2021).

[12] Qi-Fan Yang, Boqiang Shen, Heming Wang, Minh Tran, Zhewei Zhang, Ki Youl Yang, Lue Wu, Chengying Bao, John Bowers, Amnon Yariv, Kerry Vahala. Vernier spectrometer using counterpropagating soliton microcombs. *Science* **363**, 965-968 (2019).

[13] Johann Riemensberger, Anton Lukashchuk, Maxim Karpov, Wenle Weng, Erwan Lucas, Junqiu Liu & Tobias J. Kippenberg. Massively parallel coherent laser ranging using a soliton microcomb. *Nature* **581**, 164–170 (2020).

[14] Brian Stern, Xingchen Ji, Yoshitomo Okawachi, Alexander L. Gaeta & Michal Lipson. Battery-operated integrated frequency comb generator. *Nature* **562**, 401–405 (2018).

[15] Bowen Bai, Qipeng Yang, Haowen Shu, Lin Chang, Fenghe Yang, Bitao Shen, Zihan Tao, Jing Wang, Shaofu Xu, Weiqiang Xie, Weiwen Zou, Weiwei Hu, John E. Bowers & Xingjun Wang. Microcomb-based integrated photonic processing unit. *Nat. Commun.* **14**, 66 (2023).

[16] Boqiang Shen, Lin Chang, Junqiu Liu, Heming Wang, Qi-Fan Yang, Chao Xiang, Rui Ning Wang, Jijun He, Tianyi Liu, Weiqiang Xie, Joel Guo, David Kinghorn, Lue Wu, Qing-Xin Ji, Tobias J. Kippenberg, Kerry Vahala & John E. Bowers. Integrated turnkey soliton microcombs. *Nature* **582**, 365–369 (2020).

[17] Warren Jin, Qi-Fan Yang, Lin Chang, Boqiang Shen, Heming Wang, Mark A. Leal, Lue Wu, Maodong Gao, Avi Feshali, Mario Paniccia, Kerry J. Vahala & John E. Bowers. Hertz-linewidth semiconductor lasers using CMOS-ready ultra-high-Q microresonators. *Nature Photon.* **15**, 346–353 (2021)

[18] David Marpaung, Jianping Yao & José Capmany. Integrated microwave photonics. *Nature Photon.* **13**, 80–90 (2019).

[19] P. Krantz, M. Kjaergaard, F. Yan, T. P. Orlando, S. Gustavsson, and W. D. Oliver. A quantum engineer's guide to superconducting qubits. *Appl. Phys. Rev.* **6**, 021318 (2019).

[20] Alexandre Blais, Steven M. Girvin and William D. Oliver. Quantum information processing and quantum optics with circuit quantum electrodynamics. *Nature Phys.* **16**, 247 (2020).

[21] A. A. Clerk, K. W. Lehnert, P. Bertet, J. R. Petta and Y. Nakamura. Hybrid quantum systems with circuit quantum electrodynamics. *Nature Phys.* **16**, 257 (2020).

[22] Alexandre Blais, Arne L. Grimsmo, S. M. Girvin, and Andreas Wallraff. Circuit quantum electrodynamics. *Rev. Mod. Phys.* **93**, 025005 (2021).

[23] Dmitry S. Golubev, Evgeni V. Il'ichev, and Leonid S. Kuzmin. Single-Photon Detection with a Josephson Junction Coupled to a Resonator. *Phys. Rev. Applied* **16**, 014025 (2021).

[24] O.-P. Saira, M. Zgirski, K. L. Viisanen, D. S. Golubev, and J. P. Pekola. Dispersive Thermometry with a Josephson Junction Coupled to a Resonator. *Phys. Rev. Applied* **6**, 024005 (2016).

[25] M. C. Cassidy, A. Bruno, S. Rubbert, M. Irfan, J. Kammhuber, R. N. Schouten, A. R. Akhmerov, L. P. Kouwenhoven. Demonstration of an ac Josephson junction laser. *Science* **355**, 939-942 (2017).

[26] Chengyu Yan, Juha Hassel, Visa Vesterinen, Jinli Zhang, Joni Ikonen, Leif Grönberg, Jan Goetz, and Mikko Möttönen. A low-noise on-chip coherent microwave source. *Nature Electron.* **4**, 885 (2021).

[27] O. Astafiev, K. Inomata, A. O. Niskanen, T. Yamamoto, Yu. A. Pashkin, Y. Nakamura, & J. S. Tsai. Single artificial-atom lasing. *Nature* **449**, 588-590 (2007).

[28] S. Meister, M. Mecklenburg, V. Gramich, J. T. Stockburger, J. Ankerhold, and B. Kubala. Resonators coupled to voltage-biased Josephson junctions: From linear response to strongly driven nonlinear oscillations. *Phys. Rev. B* **92**, 174532 (2015).

[29] C. Rolland, A. Peugeot, S. Dambach, M. Westig, B. Kubala, Y. Mukharsky, C. Altimiras, H. le Sueur, P. Joyez, D. Vion, P. Roche, D. Esteve, J. Ankerhold, and F. Portier. Antibunched photons emitted by a dc-biased Josephson junction. *Phys. Rev. Lett.* **122**, 186804 (2019).

[30] Fei Chen, Juliang Li, A. D. Armour, E. Brahimi, Joel Stettenheim, A. J. Sirois, R. W. Simmonds, M. P. Blencowe, and A. J. Rimberg. Realization of a single-Cooper-pair Josephson laser. *Phys. Rev. B* **90**, 020506(R) (2014).

[31] M. Hofheinz, F. Portier, Q. Baudouin, P. Joyez, D. Vion, P. Bertet, P. Roche, and D. Esteve. Bright side of the Coulomb blockade. *Phys. Rev. Lett.* **106**, 217005 (2011).

[32] A. Grimm, F. Blanchet, R. Albert, J. Leppäkangas, S. Jebari, D. Hazra, F. Gustavo, J.-L. Thomassin, E. Dupont-Ferrier, F. Portier, and M. Hofheinz. Bright On-Demand Source of Antibunched Microwave Photons Based on Inelastic Cooper Pair Tunneling. *Phys. Rev. X* **9**, 021016 (2019).

[33] Steven H. Simon and Nigel R. Cooper. Theory of the Josephson junction laser. *Phys. Rev. Lett.* **121**, 027004 (2018).

[34] Lukas Danner, Ciprian Padurariu, Joachim Ankerhold, and Björn Kubala. Injection locking and synchronization in Josephson photonics devices. *Phys. Rev. B* **104**, 054517 (2021).

[35] Nathan R. Newbury and William C. Swann. Low-noise fiber-laser frequency combs. *J. Opt. Soc. Am. B* **24**, 1756-1770 (2007)

[36] A. Liehl, P. Sulzer, D. Fehrenbacher, T. Rybka, D. V. Seletskiy, and A. Leitenstorfer. Deterministic Nonlinear Transformations of Phase Noise in Quantum-Limited Frequency Combs. *Phys. Rev. Lett.* **122**, 203902 (2019).

[37] Y.-Y. Liu, J. Stehlik, M. J. Gullans, J. M. Taylor, and J. R. Petta. Injection locking of a semiconductor double-quantum-dot micromaser. *Phys. Rev. A* **92**, 053802 (2015).

[38] Y.-Y. Liu, T. R. Hartke, J. Stehlik, and J. R. Petta. Phase locking of a semiconductor double-quantum-dot single-atom maser. *Phys. Rev. A* **96**, 053816 (2017).

[39] Johannes Hillbrand, Aaron Maxwell Andrews, Hermann Detz, Gottfried Strasser and

Benedikt Schwarz. Coherent injection locking of quantum cascade laser frequency combs. *Nature Photon.* **13**, 101-104 (2018).

[40] Gellie, P. et al. Injection-locking of terahertz quantum cascade lasers up to 35 GHz using RF amplitude modulation. *Opt. Express* **18**, 20799–20816 (2010).

[41]. Barbieri, S. et al. Coherent sampling of active mode-locked terahertz quantum cascade lasers and frequency synthesis. *Nature Photon.* **5**, 306–313 (2011).

[42] St-Jean, M. R. et al. Injection locking of mid-infrared quantum cascade laser at 14 GHz, by direct microwave modulation. *Laser Photon. Rev.* **8**, 443–449 (2014).

[43] R. Adler. A study of locking phenomena in oscillators. *Proc. IRE* **34**, 351-357 (1946).

[44] R. P. Erickson, M. R. Vissers, M. Sandberg, S. R. Jefferts, and D. P. Pappas. Frequency Comb Generation in Superconducting Resonators. *Phys. Rev. Lett.* **113**, 187002 (2014).

[45] Shuai-Peng Wang, Zhen Chen, and Tiefu Li. Controllable microwave frequency comb generation in a tunable superconducting coplanar-waveguide resonator. *Chin. Phys. B* **30**, 048501 (2021).

[46] Pinlei Lu, Tzu-Chiao Chien, Xi Cao, Olivia Lanes, Chao Zhou, Michael J. Hatridge, Saeed Khan, and Hakan E. Türeci. Nearly Quantum-Limited Josephson-Junction Frequency-Comb Synthesizer. *Phys. Rev. Appl.* **15**, 044031 (2021).

[47] Junghyun Shin, Younghun Ryu, Mohammad-Ali Miri, Seung-Bo Shim, Hyoungsoon Choi, Andrea Alù, Junho Suh, and Jinwoong Cha. On-Chip Microwave Frequency Combs in a Superconducting Nanoelectromechanical Device. *Nano Lett.* **22**, 5459−5465 (2022).

[48] Sishi Wu, Yulong Liu, Qichun Liu, Shuai-Peng Wang, Zhen Chen, and Tiefu Li. Hybridized Frequency Combs in Multimode Cavity Electromechanical System. *Phys. Rev. Lett.* **128**, 153901 (2022).

[49] Xu Han, Chang-Ling Zou, Wei Fu, Mingrui Xu, Yuntao Xu, and Hong X. Tang. Superconducting Cavity Electromechanics: The Realization of an Acoustic Frequency Comb at Microwave Frequencies. *Phys. Rev. Lett.* **129**, 107701 (2022).

[50] Saeed Khan and Hakan E. Türeci. Frequency Combs in a Lumped-Element Josephson-Junction Circuit. *Phys. Rev. Lett.* **120**, 153601 (2018).

[51] P. Solinas, S. Gasparinetti, D. Golubev & F. Giazotto. A Josephson radiation comb. *Sci. Rep.* **4**, 12260 (2015).

[52] Denis Ilin, Alexander V. Poshakinskiy, Alexander N. Poddubny, and Ivan Iorsh. Frequency Combs with Parity-Protected Cross-Correlations and Entanglement from Dynamically Modulated Qubit Arrays. *Phys. Rev. Lett.* **130**, 023601 (2023).

[53] Antoine Essig, Quentin Ficheux, Théau Peronnin, Nathanaël Cottet, Raphaël Lescanne, Alain Sarlette, Pierre Rouchon, Zaki Leghtas, and Benjamin Huard. Multiplexed Photon Number Measurement. *Phys. Rev. X* **11**, 0311045 (2021).

[54] Steven t. cundiff and andrew M. Weiner. Optical arbitrary waveform generation. *Nature Photon.* **4**, 760-766 (2010).

[55] William M. Strickland, Bassel Heiba Elfeky, Joseph O'Connell Yuan, William F. Schiela, Peng Yu, Dylan Langone, Maxim G. Vavilov, Vladimir E. Manucharyan and Javad Shabani. Superconducting Resonators with Voltage-Controlled Frequency and Nonlinearity. *Phys. Rev. Appl.* **19**, 034021 (2023)

[56] L. Ozyuzer, A. E. Koshelev, C. Kurter, N. Gopalsami, Q. Li, M. Tachiki, K. Kadowaki, T. Yamamoto, H. Minami, H. Yamaguchi, T. Tachiki, K. E. Gray, W.-K. Kwok, U. Welp. Emission of Coherent THz Radiation from Superconductors. *Science* **318**, 1291-1293 (2007).

[57] Lili Shi, Tingting Guo, Runfeng Su, Tianyuan Chi, Yifan Sheng, Junliang Jiang, Chunhai Cao, Jingbo Wu, Xuecou Tu, Guozhu Sun, Jian Chen, Peiheng Wu. Tantalum microwave resonators with ultra-high intrinsic quality factors. *Appl. Phys. Lett.* **121**, 242601 (2022).

Acknowledgements

Author Contributions

Y.L.W., H.W. and P.W. conceived and supervised the project. C.G.W. designed and fabricated the devices, as well as conducted the experiments. L.S., J.J., T.G., C.C., X.J., and J.C. provided support for fabrication of resonators. T.L., Y.Y.L. and G.S. assisted in the fabrication of Josephson junctions. W.X., C.L., W.C.Y., X.T., and L.K. provided support for optical lithography. W.X., S.D., P.Z., Y.Y.L., J.P. and L.Z. assisted in microwave spectrum and waveform measurements. C.G.W. and Y.L.W. performed the analysis and interpretation of the experimental data. C.G.W., X.D., Y.D. and Y.L.W. conducted the theoretical analysis. C.G.W., and Y.L.W. wrote the manuscript. Y.L.W. and H.W. edited the manuscript.

Competing Interests
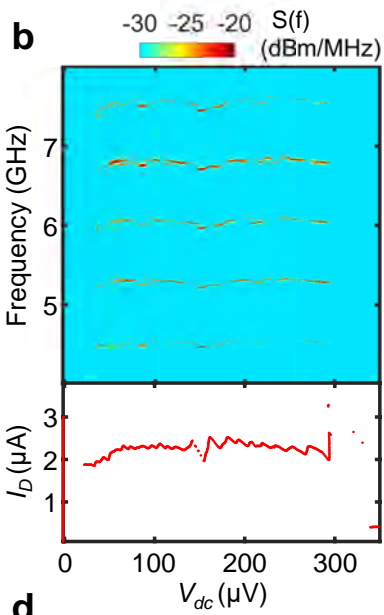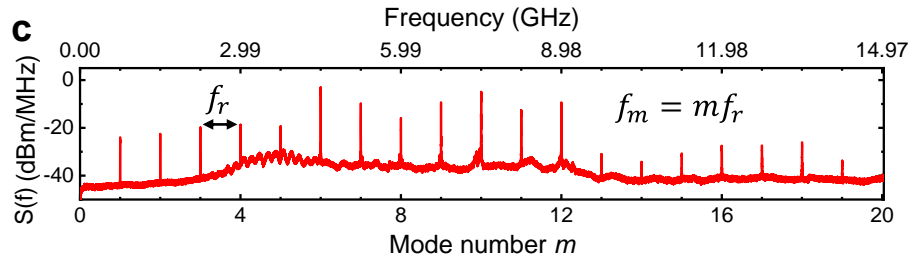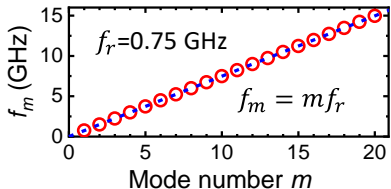
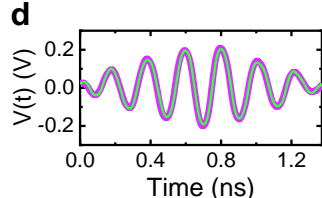The authors declare no competing interests.
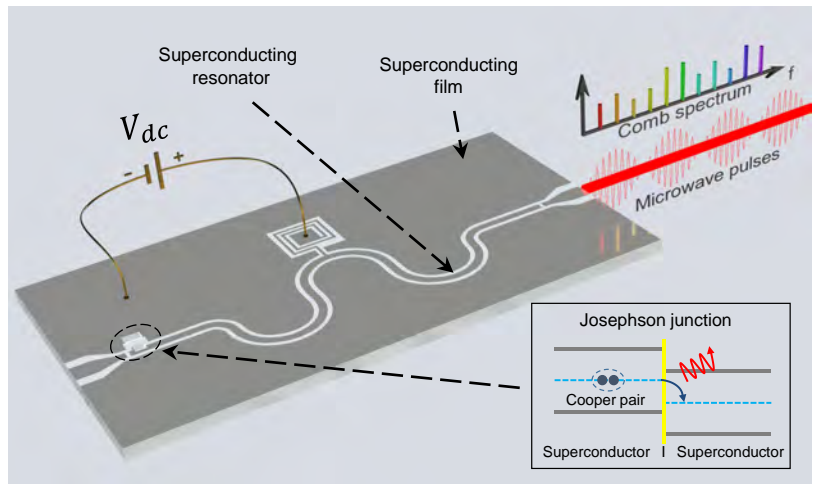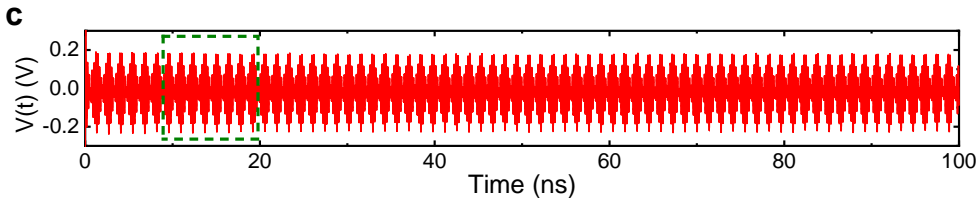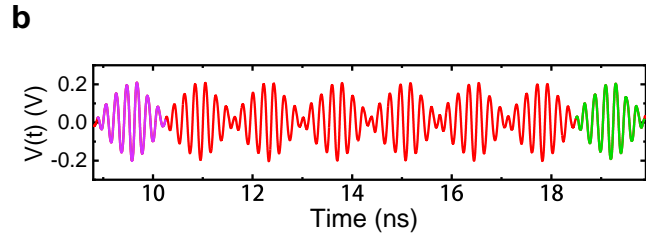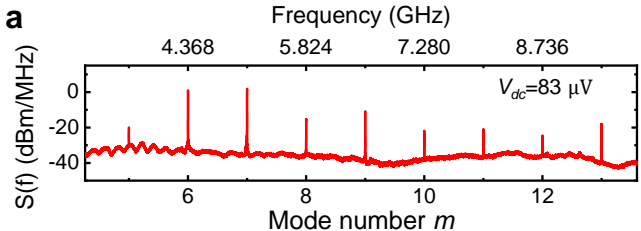
Figure legends/captions

Fig. 1 | Integrated and DC-powered superconducting microcomb. (**a**) Illustration of the device. Frequency comb emission is generated when a DC voltage-biased (V_{dc}) Josephson junction is coupled to a superconducting CPW resonator. (**b**) The power spectral density (top) and flowing supercurrent through the Josephson junction (bottom) as a function of DC bias-voltage. (**c**) Frequency comb spectrum obtained at V_{dc}=43 µV. (**d**) Extracted emission frequencies (open dots) from (c). The dashed line represents fitting to the comb formula $f_m = mf_r$.

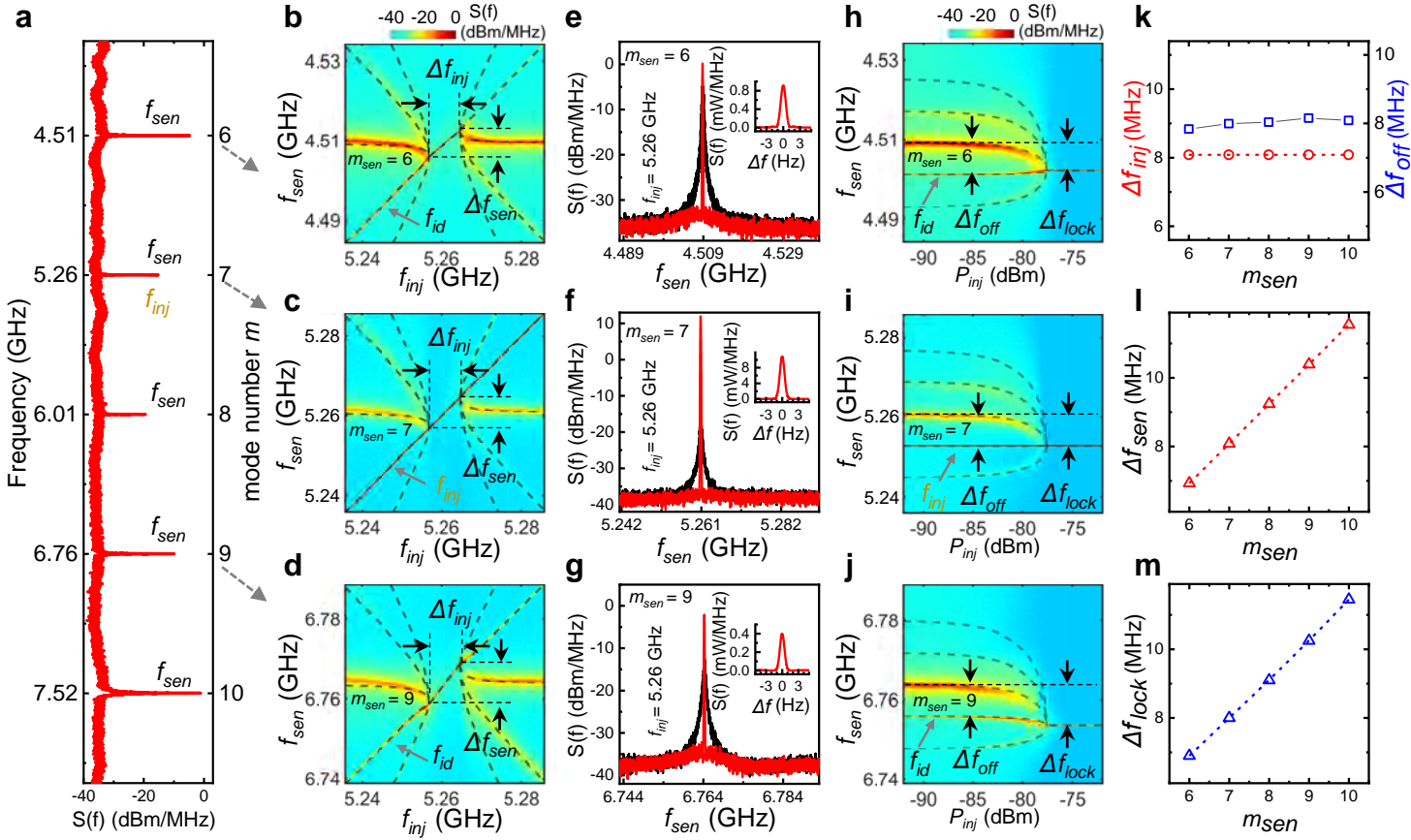**Fig. 2 | Coherent pulse-wave.** (**a**) Comb spectrum obtained at V_{dc}=83 µV. (**b-d**) Pulse waveforms corresponding to the spectrum in (a). The zoom-in waveform (b) of the region enclosed by the green-dashed box in (c) displays two highlighted pulse waves with purple and green, which overlap perfectly in (d).
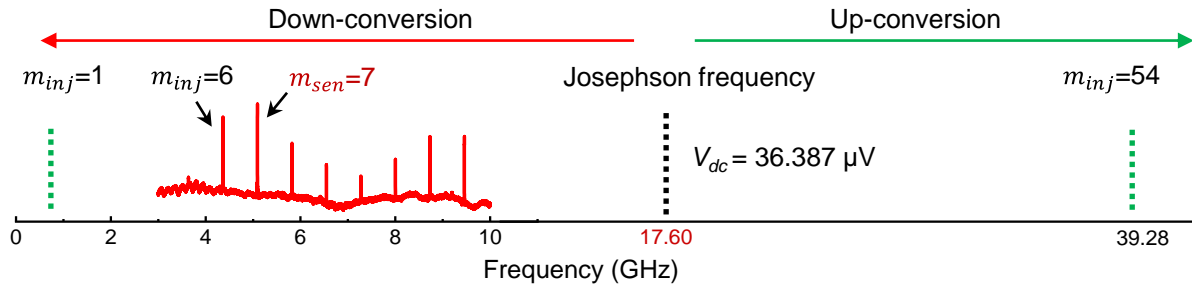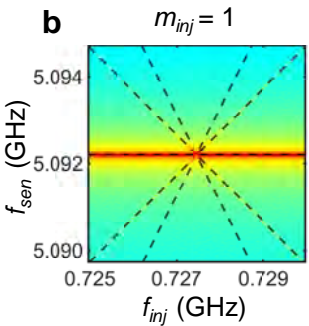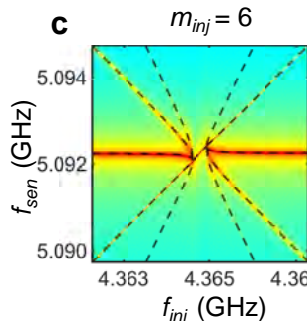
Fig. 3 | Coherent injection locking effect. (**a**) A comb spectrum showing five observed modes. (**b-d**) Spectrum maps obtained by sweeping the injection frequency f_{inj} around f_7 at a fixed power (P_{inj}=-82 dBm), and at various sensing modes m_{sen}=6 (b), 7 (c) and 9 (d), respectively. The emission signals are locked within the range Δf_{inj} and Δf_{sen}. (**e-g**) Comparison of spectra between free-running (black) and injection-locking (red) states. Insets show the linewidth, which is ≤ 1 Hz for all locked modes. (**h-j**) Spectra maps obtained by varying injection power (P_{inj}) with an off-resonance tone ($f_{inj}=f_7-\Delta f_{off}$; f_7=5.26 GHz, Δf_{off}=8 MHz). The shifts of the locked tone from the free-running tones are indicated by Δf_{lock}. The long-dashed lines in (b-d, h-j) are fittings to extended Alder's equation (2). (**k-m**) Plots of Δf_{inj} and Δf_{off} (k), Δf_{sen} (l), and Δf_{lock} (m) as functions of mode number m.

Fig. 4 | Up- and down-conversion of Josephson photons into multiple modes. (**a**) Illustration of the up- and down-conversion. A comb spectrum (red) is obtained at $V_{dc} = 36.39$ µV, corresponding to a Josephson frequency of 17.6 GHz. (**b-d**) Coherent injection locking effects with m_{sen}=7 and for injections at m_{inj}=1 (b), 6 (c), and 54 (d), respectively. The dashed lines are fittings to extended Alder's equation (2).

a

V_dc

Superconducting resonator

Superconducting film

Comb spectrum

Microwave pulses

Josephson junction

Cooper pair

Superconductor   I   Superconductor

b

$S(f)$

-30 -25 -20

(dBm/MHz)

Frequency (GHz)

I_D (μA)

V_{dc} (μV)

c

Frequency (GHz)

0.00   2.99   5.99   8.98   11.98   14.97

$S(f)$ (dBm/MHz)

f_r

$f_m = m f_r$

Mode number m

d

f_m (GHz)

$f_r = 0.75$ GHz

$f_m = m f_r$

Mode number m

a Frequency (GHz): 4.368, 5.824, 7.280, 8.736

$S(f)$ (dBm/MHz) vs Mode number m, $V_{dc} = 83$ μV

b $V(t)$ (V) vs Time (ns)

c $V(t)$ (V) vs Time (ns)

d $V(t)$ (V) vs Time (ns)

a

Down-conversion ← → Up-conversion

$m_{inj}=1$ $m_{inj}=6$ $m_{sen}=7$ Josephson frequency $m_{inj}=54$

$V_{dc}=36.387$ µV

Frequency (GHz)

0   2   4   6   8   10   17.60   39.28

b $m_{inj}=1$

f_{sen} (GHz)

f_{inj} (GHz)

c $m_{inj}=6$

f_{sen} (GHz)

f_{inj} (GHz)

d $m_{inj}=54$

Δf_{inj}

f_{sen} (GHz)

f_{inj} (GHz)

f_{sen} (GHz)

f_{inj} (GHz)

$S(f)$ (dBm/MHz)

-10

-50